Nonequilibrium chiral soliton lattice in the monoaxial chiral magnet $MnNb_3S_6$

M. Ohkuma,[1,*] M. Mito,[1,2] H. Deguchi,[1] Y. Kousaka,[2,3] J. Ohe,[4] J. Akimitsu,[2,5] J. Kishine,[2,6,7] and K. Inoue[2,8,9]

[1]*Graduate School of Engineering, Kyushu Institute of Technology, Kitakyushu 804-8550, Japan*
[2]*Chirality Research Center, Hiroshima University, Higashihiroshima 739-8526, Japan*
[3]*Department of Physics and Electronics, Osaka Prefecture University, 1-1 Gakuencho, Sakai, Osaka 599-8531, Japan*
[4]*Department of Physics, Toho University, Funabashi, Chiba 274-8510, Japan*
[5]*Research Institute for Interdisciplinary Science, Okayama University, Okayama 700-8530, Japan*
[6]*Division of Natural and Environmental Sciences, The Open University of Japan, Chiba 261-8586, Japan*
[7]*Institute for Molecular Science, 38 Nishigo-Naka, Myodaiji, Okazaki 444-8585, Japan*
[8]*Graduate School of Advanced Science and Engineering, Hiroshima University, Higashihiroshima 739-8526, Japan*
[9]*Institute for Advanced Materials Research, Hiroshima University, Higashihiroshima 739-8526, Japan*

(Received 23 December 2021; revised 16 August 2022; accepted 22 August 2022; published 13 September 2022)

In a magnetic superlattice composed of kinks in a ferromagnetic spin array, the change in the kink number requires the movement of the kinks to and from the crystal surface. Namely, the kinks must have a velocity, and the superlattice must be nonequilibrium. Evidence of the nonequilibrium state has never been observed in previous model compounds. In $MnNb_3S_6$, a long magnetization relaxation was observed, and the nature of the nonequilibrium state was more pronounced in the kink annihilation process rather than the kink creation process. The annihilation process can be phenomenologically reproduced using the unfrustrated magnetic clusters model. The nonequilibrium state in the annihilation process has a longer relaxation time than that in the nucleation process, since an energy barrier exists only in the latter.

DOI: 10.1103/PhysRevB.106.104410

I. INTRODUCTION

Recently, topological objects in the spin systems, such as vortices termed as magnetic skyrmions and kinks termed as magnetic solitons, have attracted attention in fundamental physics and applications [1–5]. They can be stabilized in various magnetic materials with different types of interactions. Some of these magnets are noncentrosymmetric bulk magnets that exhibit either left-handed or right-handed chiral helimagnetic (CHM) structures owing to the Dzyaloshinskii-Moriya (D–M) interaction [6,7]. These magnets exhibit emergent physical phenomena that originate from nontrivial topological spin textures [8,9]. In particular, a chiral soliton lattice (CSL), when stabilized by applying a magnetic field (H) perpendicular to the helical axis, exhibits characteristic transport and magnetic properties accompanying the change in the number of magnetic kinks, which are termed as solitons [10]. When the applied H is greater than the critical magnetic field (H_c), the forced ferromagnetic state (FFM), whose magnetic moments are aligned in the direction of H, is stabilized [Fig. 1(a)].

A series of experimental and theoretical studies on the archetypical monoaxial chiral magnet $CrNb_3S_6$ reveals a variety of physical properties: $CrNb_3S_6$ has a CHM state along the c axis with period of 48 nm below the transition temperature ($T_c = 127$ K) [3,11]. Experiments using Lorentz transmission electron microscopy (TEM) revealed the evolution of the CSL state on $CrNb_3S_6$ under H, which is consistent with theory [3]. The magnetoresistance (MR) also shows a behavior that reflects the period of the CSL [9]. The magnetization (M) and MR show discrete changes accompanying changes in soliton number [12–16]. In the annihilation process, the solitons dissipate perpendicularly to the D–M vector toward the surface [15,16]. However, in the nucleation process, the solitons nucleate at the surface and penetrate the interior of the crystal parallel to the D–M vector [14–19]. The soliton number changes dynamically in both the annihilation and nucleation processes; however, the nonequilibrium phenomenon due to the CSL formation has not been observed experimentally.

$MnNb_3S_6$ has the crystal structure of the noncentrosymmetric hexagonal space group $P6_322$, similar to $CrNb_3S_6$ shown in Fig. 1(b) and is expected to stabilize the CHM and CSL states along the c axis [20,21]. The lattice constants of $MnNb_3S_6$ are $a = 5.78$ Å and $c = 12.61$ Å. Some of the authors previously reported M measurements on a single crystal of $MnNb_3S_6$, whose M curves were similar to those of $CrNb_3S_6$ [20]. The magnetic structure has been studied through Lorentz TEM and neutron diffraction measurements, and the measurements suggested that the distorted helimagnetic state at $H = 0$ is stable with a period of a few hundred nanometers [22,23]. Recently, Hall *et al*. proposed that the magnetic structure is a conventional ferromagnetic domain structure through Lorentz TEM measurements [24]. In this study, we examined the CSL formation and nonequilibrium phenomenon resulting from the CSL formation on a single crystal of $MnNb_3S_6$ through magnetic measurements. We observed M curves that were similar to those of $CrNb_3S_6$.

*m108022m@mail.kyutech.jp

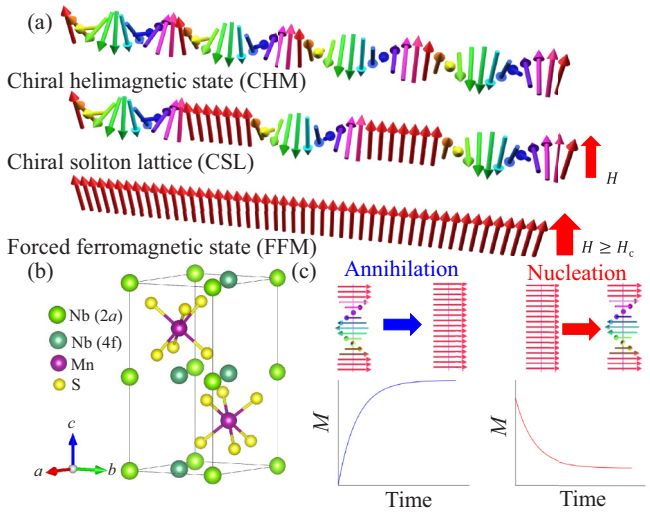

FIG. 1. (a) Magnetic structure of monoaxial chiral magnets in a magnetic field (H), chiral helimagnetic (CHM) state [top, at $H = 0$], chiral soliton lattice (CSL) [middle, $0 < H < H_c$], forced ferromagnetic state [bottom, $H \geqq H_c$]. (b) Crystal structure of $MnNb_3S_6$. (c) General idea of the magnetization (M) relaxation due to soliton annihilation and soliton nucleation in CSL.

Additionally, we observed the long-time M relaxation accompanying both the annihilation and nucleation processes.

II. PHENOMENOLOGICAL ANALYSIS ON MAGNETIC RELAXATION

In a monoaxial chiral magnet at $H = 0$ Oe, the spins rotate at a uniform angle, which is determined by the ratio of exchange interaction to D–M interaction, along the helical axis [10]. In CSL, solitions without a net moment are periodically arranged in the FFM structure. When the soliton annihilates or nucleates, the net moment increases or decreases. The annihilation and nucleation of the solitons occur only at the crystal surface, so that the solitons inside the crystal dissipate to the surface in the annihilation process and penetrate the surface in the nucleation process. Thus, the time dependence of the M behavior, as shown in Fig. 1(c), should be observed in the annihilation and nucleation processes. In this section, we briefly review the slow magnetic relaxation phenomenon.

Considering the probability of a single excitation from one energy minimum to the other during the relaxation of the thermoremanent magnetization (M_r), the relaxation phenomenon can be described by a simple exponential function:

$$M_r(t) = M_r(0)e^{-t/\tau}, \tag{1}$$

where $M_r(0)$ and τ are the initial magnetization and the relaxation time, respectively. However, in some complex magnetic materials such as spin glass materials, the relaxation phenomenon can not be described by Eq. (1) but by using substitute functions such as the stretched exponential function [25] or the power law [26] which are given as follows:

$$M_r(t) = M_r(0)\exp[-(t/\tau)^{\beta}], \tag{2}$$

$$M_r(t) = M_r(0)t^{-\alpha}, \tag{3}$$

where β and α are constants. The relaxation of the zero-field-cooled and field-cooled M [$M(t)$] is often described by the stretched exponential form in some spin glass materials [27–29]. For a magnetic cluster system in a two-dimensional networked single-molecular magnet (SMM), wherein the magnetic moments of each SMM form a cluster, the magnetic relaxation behavior exhibits nonexponential slow dynamics according to the following equation [30,31]:

$$M_r(t) = M_r(0)\exp[-c(\ln t)^{d/(d-1)}], \tag{4}$$

where c and d are the decay constant and system dimension, respectively. This equation was first introduced by Randeria *et al*. for the Griffiths phase in randomly diluted Ising ferromagnets [32–34], wherein the spin-flip dynamics of unfrustrated magnetic clusters resulted in nonexponential relaxation.

No theoretical study has been conducted on the magnetic relaxation of the soliton in the CSL state. In contrast, the decay of the metastable skyrmions, which is stabilized using field cooling methods in cubic chiral magnets, has been experimentally investigated [35–38]. These relaxation phenomena were reproduced by a simple exponential function in the case of MnSi and $Fe_{1-x}Co_xSi$ [35,36], or a stretched exponential function in the case of Co-Mn-Zn alloys and Cu_2OSeO_3 [37–39]. In a CSL state on a monoaxial chiral magnet, we must identify the model that is phenomenologically the most suitable for reproducing the magnetic relaxation of the soliton. If each soliton annihilates independently, then the relaxation behavior may be decsribed using Eq. (2). However, in our idea, the change in solitons in the sea of ferromagnetic moments should be analyzed based on the dynamics of soliton aggregates. If solitons annihilate as aggregates, then the magnetic relaxation would be reproduced by Eq. (4). In this study, we analyzed $M(t)$ for the following CSL material $MnNb_3S_6$ with four models; consequently, we demonstrated that just after changing H, $M(t)$ exhibits the nonequillibrium state. The experimental results are compared with those of a typical monoaxial chiral magnet, $CrNb_3S_6$.

III. EXPERIMENTAL PROCEDURES

The powder sample and single crystals of $MnNb_3S_6$ and $CrNb_3S_6$ were synthesized using a procedure described elsewhere [20]. We obtained the single crystal of $MnNb_3S_6$ whose M-H curves were similar to those of the CSL state. The dimensions of the single crystal of $MnNb_3S_6$ were 1.3 mm^2 of ab plane and 70 μm along the c axis.

M and both in-phase and out-of-phase components of ac magnetization (m' and m'') were observed using a superconducting quantum interference device (SQUID) magnetometer (Quantum Design Inc.) equipped with an ac measurement option. The frequency f and amplitude h of the ac magnetic field (H_{ac}) were 1–100 Hz and 3.9 Oe, respectively.

We calculated the M dynamics by changing H [15,16]. The M dynamics obey the Landau-Lifshitz-Gilbert equation,

which is given by

$$\frac{\partial \boldsymbol{M}}{\partial t} = -\gamma \boldsymbol{M} \times \boldsymbol{H}_{\rm eff} + \frac{\alpha}{M_{\rm s}}\left(\boldsymbol{M} \times \frac{\partial \boldsymbol{M}}{\partial t}\right), \tag{5}$$

where $\boldsymbol{M}$ is the magnetization, γ is the gyromagnetic ratio, and $\alpha\ (=0.05)$ is the Gilbert damping coefficient. $M_{\rm s}\ (=0.1$ T) denotes the saturation magnetization. $\boldsymbol{H}_{\rm eff}$ is the effective magnetic field obtained by $\boldsymbol{H}_{\rm eff} = -\frac{\partial E}{\partial \boldsymbol{M}}$, where E is the total energy of the spin system including the ferromagnetic exchange coupling, D–M interaction, and H. We used a two-dimensional square lattice with the lattice constant $a = 1$ nm, and magnetization curves were calculated for a system landscape containing 300×30 unit cells. The exchange energy along the c axis ($J^{\parallel}$) was 7.0 K and 56 K along the in-plane direction ($J^{\perp}$). The energy of D–M interaction was 0.88 K ($J^{\parallel}/D \sim 8$), the magnetization curve was obtained by varying H (at a ratio of 100 Oe/ns). We introduced the finite temperature effect using the random magnetic field $\boldsymbol{H}_{\rm temp}$. $\boldsymbol{H}_{\rm temp}$ satisfies $\langle H^{\eta}_{\rm temp}(t) H^{\kappa}_{\rm temp}(t')\rangle = \frac{2\alpha k_{\rm B} T}{M_{\rm s}}\delta_{\eta\kappa}\delta(t-t')$, where η and κ are Cartesian coordinates.

IV. EXPERIMENTAL RESULTS

A. Temperature dependence

Figure 2(a) shows the T dependence of M under H. A small peak-like anomaly was observed at approximately 42 K in M at $H = 10$ Oe, corresponding to the transition from the CHM state to the paramagnetic state. As shown in Fig. 2(b), the T dependence of m' at zero field exhibits a small peak-like anomaly around 42 K. This kink behavior on M-T is in good agreement with the theoretical calculation based on the sine-Gordon model [40]. The $T_{\rm c}$ value is consistent with previous studies [20,22,41–43]. In contrast, the T dependence of m'' displayed the complex behavior. m'' slightly increased with increasing T around 13 K, after which it demonstrated a local maximum around 30 K. Subsequently, the m'' displayed sharp peak behavior at $T_{\rm c}$ and small peak behavior around 48 K, which was higher than $T_{\rm c}$. This result suggests any changes in the magnetic structure or magnetic domains as a function of T at zero field, however, it is not clear at the present stage. We measured the T dependence of both m' and m'' by varying f between 1–100 Hz; however, there no significant f dependency was observed (for details, see Supplemental Material [44]). There is not observed glassy phenomenon, and it is reasonable to consider the T dependence of m'' as the change in the static magnetic behavior.

B. Magnetization process

To confirm the formation of CSL on $MnNb_3S_6$, we measured the M process with H perpendicular to the helical axis. Figure 3(a) shows the M-H curve at 5 K between 0 and 500 Oe with H perpendicular to the c axis. The labels $H_{\rm c1}$ and $H_{\rm c2}$ on the curve were determined using the derivative of M (dM/dH). On the figure, $H_{\rm c}$ indicates the H below which hysteresis appears. In the increasing H process, M exhibited an upward convex curvature below $H_{\rm c1}$ and subsequently showed a rapid increase between $H_{\rm c1}$ and $H_{\rm c2}$, then gradually saturated toward $H_{\rm c}$. This behavior is similar to that of the characteristic M-H curves for $CrNb_3S_6$. The M-H curves between 5–38 K

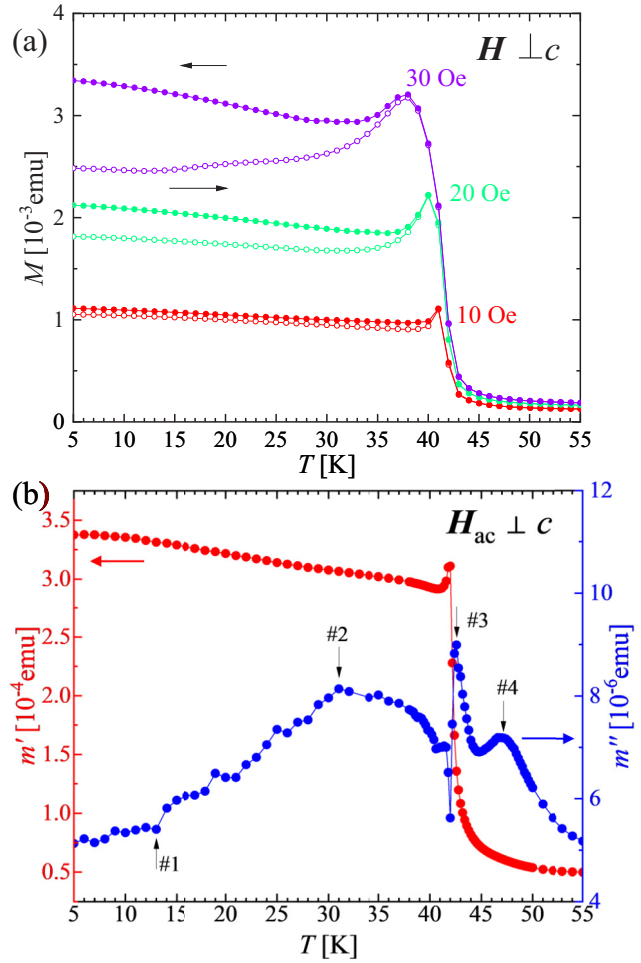

FIG. 2. (a) T dependence of the M of a single crystal of $MnNb_3S_6$. (b) T dependence of m' and m'' of a single crystal of $MnNb_3S_6$.

are shown in Fig. 3(b). For comparison, the M was normalized saturation magnetization ($M_{\rm s}$) for each T. Both the values of $H_{\rm c1}$ and $H_{\rm c2}$ shifted toward lower H side for increasing T, as shown in the inset of Fig. 3(b). We did not observed the prominent discrete changes due to the avalanche soliton nucleation in M during the decreasing H process, which has been observed in $CrNb_3S_6$ with bulk and submillimeter-sized crystals [13,16,45,46]. The inset of Fig. 3(a) shows the crystal size along c axis ($L_{\rm c}$) dependence of the magnetic hysteresis area at 5 K calculated by $M/M_{\rm s}$ as a function of $H/H_{\rm c}$. The M-H curve had a large hysteresis, as observed in $CrNb_3S_6$, whose crystal size along the c axis was a few micrometers [15,47], despite the bulk single crystal. This indicates that the total number of solitons in $MnNb_3S_6$ is as small as several hundred, because of the long helical period, as previously suggested [22,23].

For reference, the results for $H \parallel c$ axis are presented to verify that the given crystal belongs to a CHM material. When H is applied parallel to the helical c axis, a chiral conical state appears. The magnetic moments that lie in the ab-plane incline gradually toward the direction of c axis with increasing H. In the conical state, M displays a linear increase with

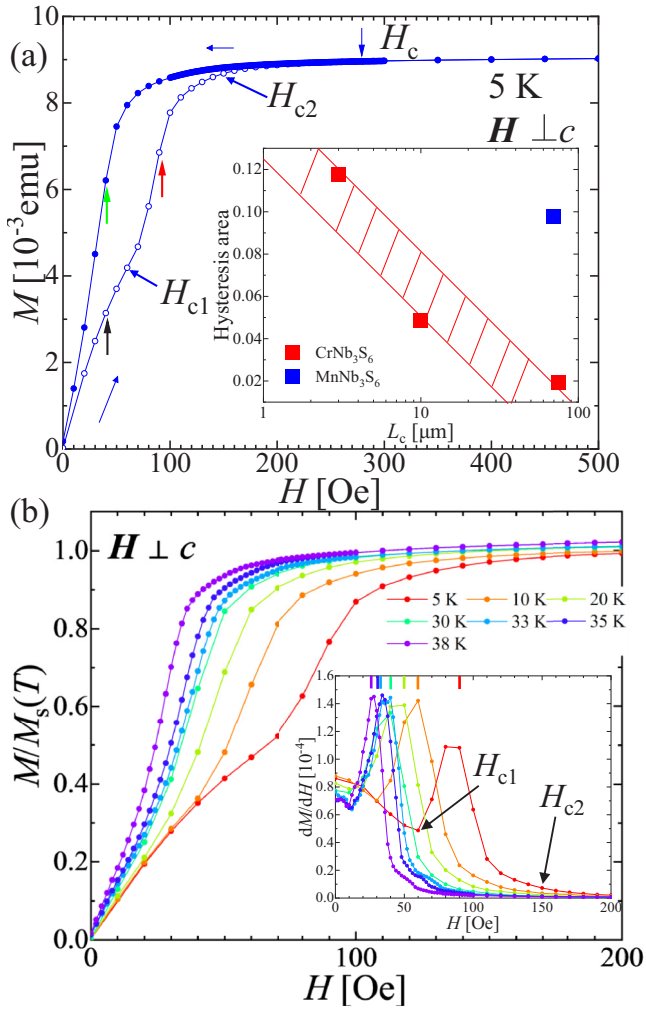

FIG. 3. (a) M-H curve with H perpendicular to the c axis on a single crystal of $MnNb_3S_6$ at 5 K. The open and closed circles represent the data of increasing H and decreasing H processes, respectively. The upward arrows indicate the H at which the magnetization relaxation measurements were carried out. The inset of panel (a) shows the crystal size along c axis (L_c) dependence of the magnetic hysteresis area at 5 K calculated by M/M_s as a function of H/H_c. The red squares indicate the magnetic hysteresis of $CrNb_3S_6$ [16,47]. (b) $M/M_s(T)$-H curve in the increasing H process at several T. The inset of panel (b) shows the H dependence of the dM/dH. The bars at the top of the inset indicate the H at which we conducted magnetization relaxation measurements.

respect to H below H_c [11]. Figure 4 shows the M-H curve at 5 K between 0 and 60 kOe with H parallel to the c axis. M varies almost linearly below 30 kOe, and there is no magnetic hysteresis. This behavior has not been observed in previous M measurements on $MnNb_3S_6$ [22,42], and it validates that the CHM state is stabilized in our single crystal.

To understand M relaxation in $MnNb_3S_6$, the phase diagram as a function of T and H is crucial. Figure 5 shows the magnetic phase diagram of the $MnNb_3S_6$ single crystal obtained by magnetization process with increasing H. H_{c1} increases with decreasing T in the vicinity of T_c after which it attains an almost constant value between 15 and 30 K. Below

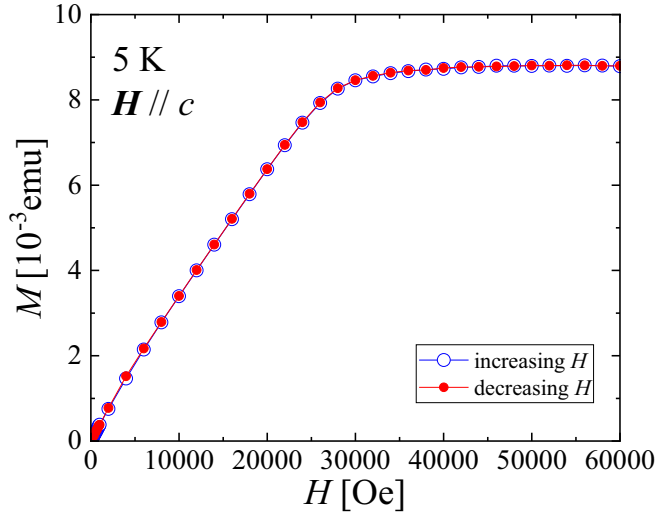

FIG. 4. M-H curve with H parallel to the c axis on a single crystal of $MnNb_3S_6$ at 5 K. The blue open and red closed circles represent the data of increasing H and decreasing H processes, respectively.

15 K, H_{c1} displayed an exponential increase with decreasing T. This behavior was not observed in $CrNb_3S_6$ [9,48,49]. We assume that the aforementioned property may have originated from the change in the Jahn-Teller distortion of the Mn system.

C. Magnetization relaxation

In this section, we present details regarding the M relaxation measurements. The H values at which we measured time evolution of M were shown in Fig. 5 as blue open circles. They are also presented by upward arrows in Fig. 3(a) and by bars in the inset of Fig. 3(b) (for details, see Supplemental Material [44]). The long-time M relaxation was observed only when the value of H was between H_{c1} and H_{c2}.

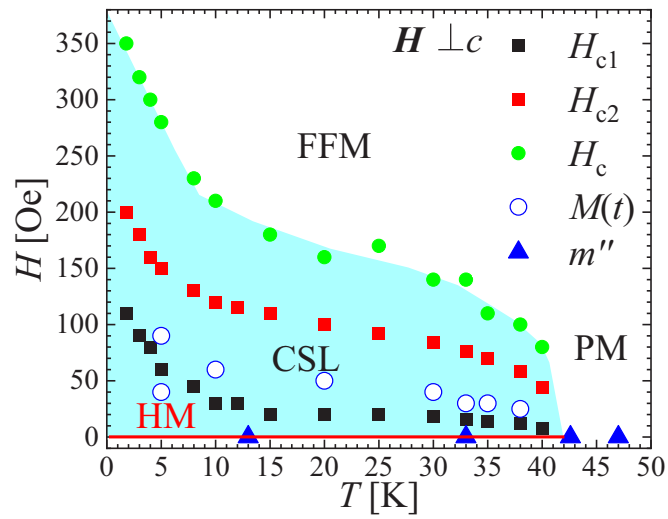

FIG. 5. Magnetic phase diagram of $MnNb_3S_6$ single crystal. Blue open circles termed $M(t)$ indicate the H at which we conducted the magnetization relaxation measurements.

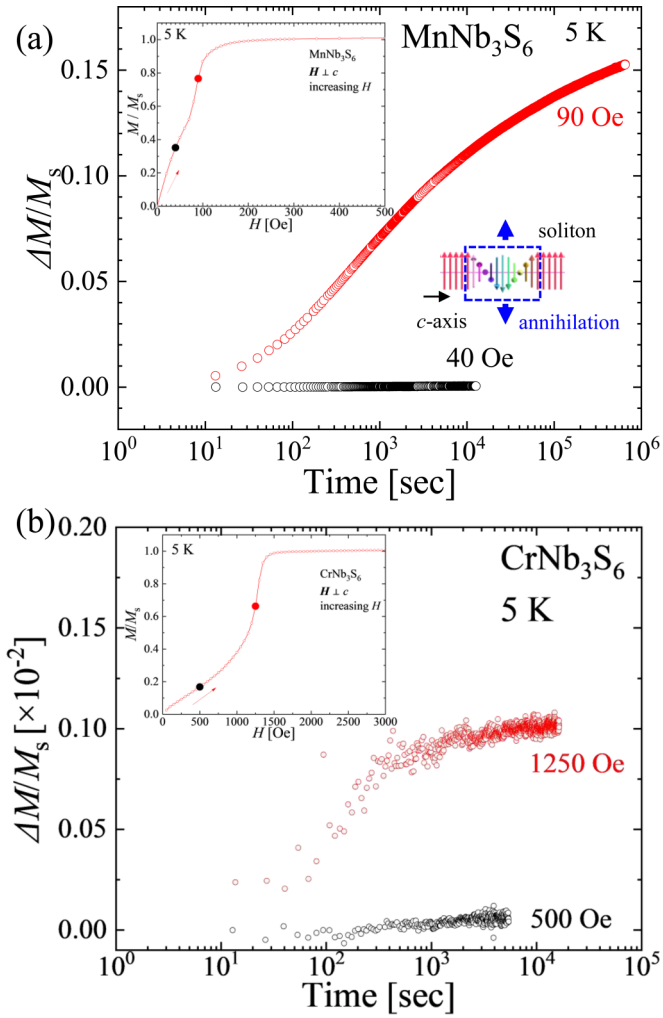

FIG. 6. (a) Time evolution of magnetization on $MnNb_3S_6$ single crystal. H was set between H_{c1} and H_{c2} (90 Oe) or below H_{c1} (40 Oe) with increasing H, as shown in the inset of panel (a), which represents the M-H curve at 5 K. (b) Time evolution of magnetization on $CrNb_3S_6$ single crystal. H was set between H_{c1} and H_{c2} (1250 Oe) or below H_{c1} (500 Oe) with increasing H, as shown in the inset of panel (b), which represents the M-H curve at 5 K.

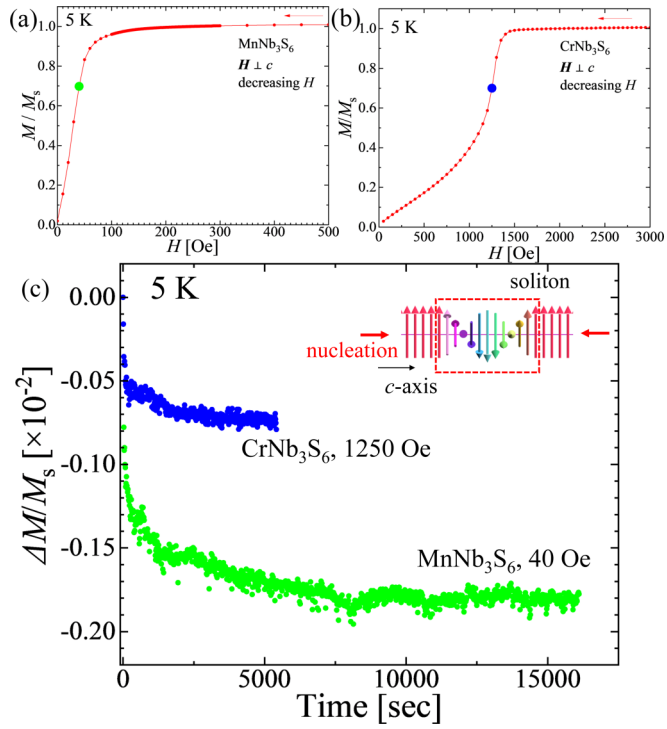

FIG. 7. (a) M-H curve in the decreasing H process with H perpendicular to the c axis on a single crystal of $MnNb_3S_6$ at 5 K. (b) M-H curve in the decreasing H process with H perpendicular to the c-axis on a single crystal of $CrNb_3S_6$ at 5 K. (c) Time evolution of magnetization on $MnNb_3S_6$ and $CrNb_3S_6$ single crystals. H was set at 40 Oe for $MnNb_3S_6$ and at 1250 Oe for $CrNb_3S_6$ with decreasing H, as shown in panels (a) and (b).

Figure 6(a) shows the M normalized by M_s as function of time at 5 K for the increasing H process on $MnNb_3S_6$ single crystal. In the measurements of the time evolution of M, we traced the changes from the first data in M [$\Delta M \equiv M(t) - M(0)$] after stabilizing H. The H at which we conducted M relaxation measurements are shown in the inset of Fig. 6(a). At $H = 90$ Oe for the increasing H process, which is between H_{c1} and H_{c2}, a long-time M relaxation was observed. The growth of M reached almost 16% of M_s. However, at $H = 40$ Oe, which was below H_{c1}, a significant magnetization relaxation was not observed (at most 0.05%). A long-time magnetization relaxation was only observed during H_{c1} and H_{c2}, where the solitons prominently annihilated. The soliton annihilation process is not completed even after H stabilizes, probably because of the long-range CHM ground state.

For reference, we also measured the time evolution of M on the $CrNb_3S_6$ single crystal with $T_c = 127$ K, as shown in Fig. 6(b). The H values at which we conducted magnetization relaxation measurements are shown in the inset of Fig. 6(a). In the case of $CrNb_3S_6$, the long-time M relaxation was also observed when the applied value of H was between H_{c1} and H_{c2}. The growth of M, however, was two orders of magnitude smaller than that in $MnNb_3S_6$. It is emphasized that the nonequilibrium phenomenon observed here is the intrinsic behavior in the monoaxial chiral magnet.

Figure 7(c) shows M_s as a function of time at 5 K in the decreasing H process for $MnNb_3S_6$ and $CrNb_3S_6$ single crystals. The values of H at which the measurements were conducted are shown in Figs. 7(a) and 7(b) (for details, see Supplemental Material [44]). We set the H down from 1000 Oe for $MnNb_3S_6$ and from 3000 Oe for $CrNb_3S_6$. The magnitude in the decay of M was in the same order for two chiral magnets, whereas it was two orders of magnitude smaller than the growth of M in the annihilation process for $MnNb_3S_6$. The nonequilibrium state in the annihilation process has a longer relaxation time than that in a nucleation process, as an energy barrier exists only in the latter.

Next, let us examine that the magnetization relaxation is due to the soliton annihilation. In the vicinity of T_c, the thermal fluctuation is expected to cause random soliton annihilation. Figure 8(a) shows M normalized by M_s as function of time at 33–38 K under H. H was set between H_{c1} and H_{c2} from zero at each T. For instance, the magnetization relaxation curve at 33 K first exhibited the growth of M, and

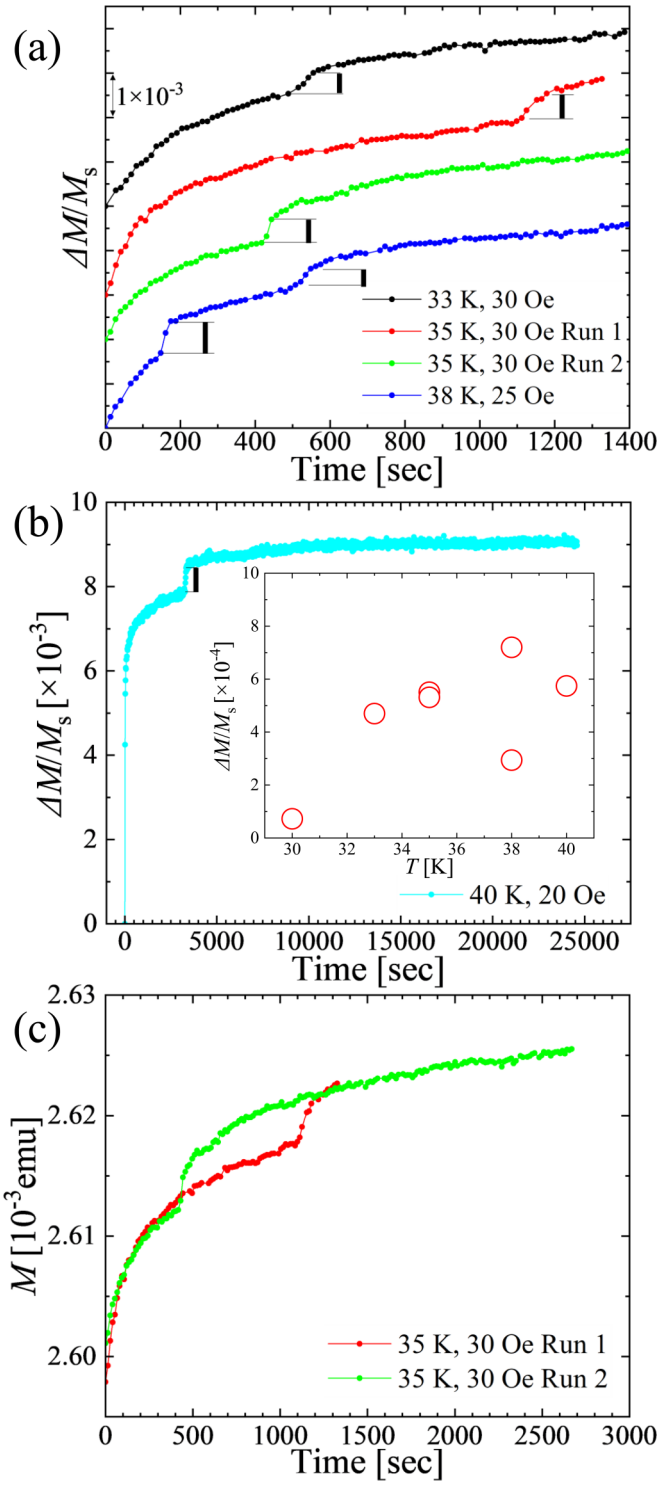

FIG. 8. (a) Time evolution of M for the increasing H processes on $MnNb_3S_6$ single crystal between 33 and 38 K. (b) Time evolution of M at 20 Oe for the increasing H process on $MnNb_3S_6$ single crystal at 40 K. The inset shows the change in $\Delta M/M_s$ due to the annihilation of the additional soliton. In panel (c), two data at 35 K, presented in panel (a), are compared. The vertical axis replaces the measured value of M.

the slope gradually decreased. Around 500 s, the slope of M changed abruptly. This behavior can be understood as indicating the annihilation of the additional soliton owing to thermal fluctuations. Figure 8(b) shows the result at 40 K. Comparing the results between 33–38 K, the initial growth of M was more prominent. This indicates that most solitons begin to annihilate simultaneously due to the thermal fluctuations during the initial relaxation process. Following this, the annihilation of surviving solitons was also observed around 3000 s, after which it gradually saturated around 10 000 s.

The black bars in Figs. 8(a) and 8(b) indicate the change in $\Delta M/M_s$ due to the annihilation of the additional soliton. We also observed minimal soliton annihilation at 30 K (for details, see Supplemental Material [44]). The changes at 35 K due to the annihilation of the additional soliton was almost same with two runs. At 38 K, the change during the first soliton annihilation was larger than that during the second soliton annihilation. The value of $\Delta M/M_s$ tends to increase with increasing T, as shown in the inset of Fig. 8(b).

Figure 8(c) shows the time evolution of M at 35 K, which is same as the data shown in Fig. 8(a). Comparing the two results, the vertical axis replaces the measured value of M. The values of M at 0 s were slightly different because there was an error in the actual H value. The behavior of two runs was almost same for $t \leqq 420$ s. The additional soliton annihilation occurred around 1100 s in Run 1 and around 430 s in Run 2, after which the M gradually increased. The values of M in Run 1 and Run 2 were almost same after the occurrence of additional soliton annihilation. The above results reveal that a soliton annihilates in the vicinity of T_c, which is an accidental phenomenon occurring due to the thermal fluctuations. The CSL state eventually settles in the same stable state when measurements are conducted under the same conditions.

V. DISCUSSION

A. Micromagnetic simulation

We performed micromagnetic simulations using the Landau-Lifshitz-Gilbert equation. Figure 9(a) shows the calculated $\Delta M/M_s$ as a function of time. The inset shows the M-H curve obtained from the calculation. At $H = 700$ Oe, which is between H_{c1} and H_{c2}, magnetic relaxation accompanying the annihilation of the soliton was observed. The growth of M reached approximately 23% of M_s, and finally, the CSL transformed to the FFM state. This behavior was not observed below H_{c1}. The snapshots of M at each time for $H = 700$ Oe are shown in Fig. 9(c). Some solitons had already started to annihilate at 0 ns because $H = 700$ Oe was larger than H_{c1}. The slope of $\Delta M/M_s$ changed slightly below the FFM state, as shown in Fig. 9(b). Comparing the snapshot of the M configuration, one can see that the slope of $\Delta M/M_s$ changes immediately after the remaining soliton starts to annihilate. This behavior is due to the finite temperature effect and is qualitatively consistent with that observed experimentally in Fig. 8. Once the dislocation was created in the remaining soliton by thermal fluctuation, the remaining soliton lost the topological stability and started to annihilate. We note that the aforementioned phenomenon does not occur when the calculation is conducted under absolute zero temperature conditions. We also performed the calculation by changing the $J^{\parallel}/D$ assuming the case of $CrNb_3S_6$. Indeed, we obtained a similar phenomenon at the higher temperature regime. Thus,

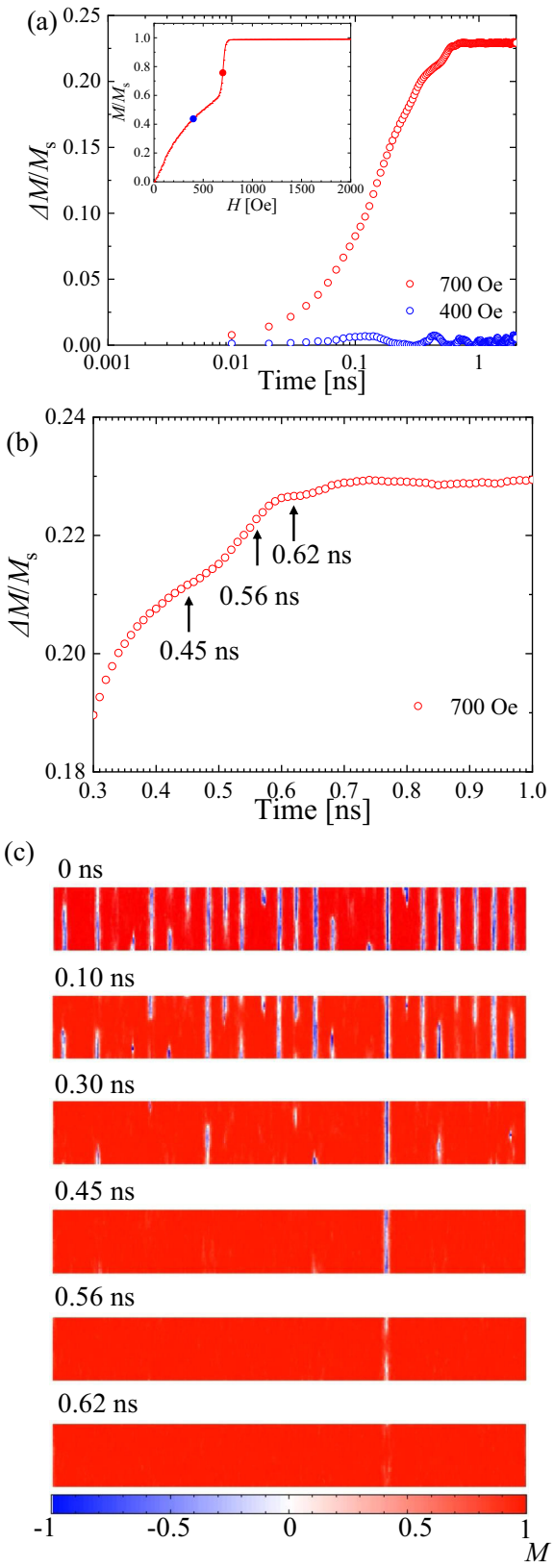

FIG. 9. (a) Time evolution of the M calculated by the Landau-Lifshitz-Gilbert equation. The inset shows the M-H curve obtained from the calculation. (b) Time evolution of M around the FFM state. (c) Snapshot of M at a certain time under a constant $H = 700$ Oe.

the M relaxation observed in $MnNb_3S_6$ would be the universal phenomenon in the CSL system.

B. Characterization of relaxation process

The experimentally observed magnetic relaxation is similar to that observed in metastable skyrmion states on cubic chiral magnets, which can be described by simple or stretched exponential functions [35–39]. Figure 10(a) shows the M normalized by M_s as function of time at 5–30 K under H on $MnNb_3S_6$. H was set between H_{c1} and H_{c2} from zero at each T. The dashed lines in Fig. 10(a) represent the result of fitting a stretched exponential function, which is given by

$$\Delta M(t) = \Delta M(\infty)\exp[-(t/\tau)^{\beta}], \tag{6}$$

where $M(\infty)$ is the equilibrium magnetization. This fitting does not show good agreement with the experiments for times less than 10^3 s. The parameters of the fitting are shown in the Supplemental Material [44]. Now, we tried to fit the magnetization relaxation to Randeria's equation as the following formula:

$$\Delta M(t) = \Delta M(\infty)\{1 - \exp[-c(\ln t)^{d/(d-1)}]\}. \tag{7}$$

The solid lines in Fig. 10(a) are the fittings of Eq. (7), and they showed good agreement with the experiments. For times greater than 10^3 s, fitting the results using Eqs. (6) and (7) presents good agreement with the experimental results. However, Randeria's equation well reproduces the experiments for times less than and greater than 10^3 s, as shown in Fig. 10(b). This reveals that the solitons in the CSL states annihilate as the aggregates of solitons. We fitted the results for $CrNb_3S_6$ using Eqs. (6) and (7), as shown in Fig. 10(c). Randeria's equation exhibits satisfactory reproduction of the experimental data over a wide time scale, similar to the case of $MnNb_3S_6$. Figure 11(a) shows T dependence of $\Delta M(\infty)/M_s$ and decay index. The fitting parameter is shown in the Supplemental Material [44].

The parameter of d at each T was 1.65–1.68 for $MnNb_3S_6$ and 1.55 for $CrNb_3S_6$ as shown in Fig. 11(b), which was close to two-dimensional. These values are consistent with the feature that the soliton annihilates perpendicular to the c axis (along the ab plane), as shown in Fig. 12. The solitons in the CSL state can be considered as a kind of magnetic cluster such that the long magnetization relaxation observed in $MnNb_3S_6$ can be phenomenologically understood as the slow spin-flip dynamics. For clusters in the Griffiths phase, the compact clusters are those with the longest relaxation times [34]. The slow relaxation for time less than 10^3 s is characteristic, probably because the solitons corresponds to the compact clusters.

C. Difference between $CrNb_3S_6$ and $MnNb_3S_6$

The long-time magnetization relaxation accompanying the annihilation of the soliton was observed in both $MnNb_3S_6$ and $CrNb_3S_6$. However, the nonequilibrium state in annihilation process for $MnNb_3S_6$ was more remarkable than that for $CrNb_3S_6$. An important difference between $CrNb_3S_6$ and

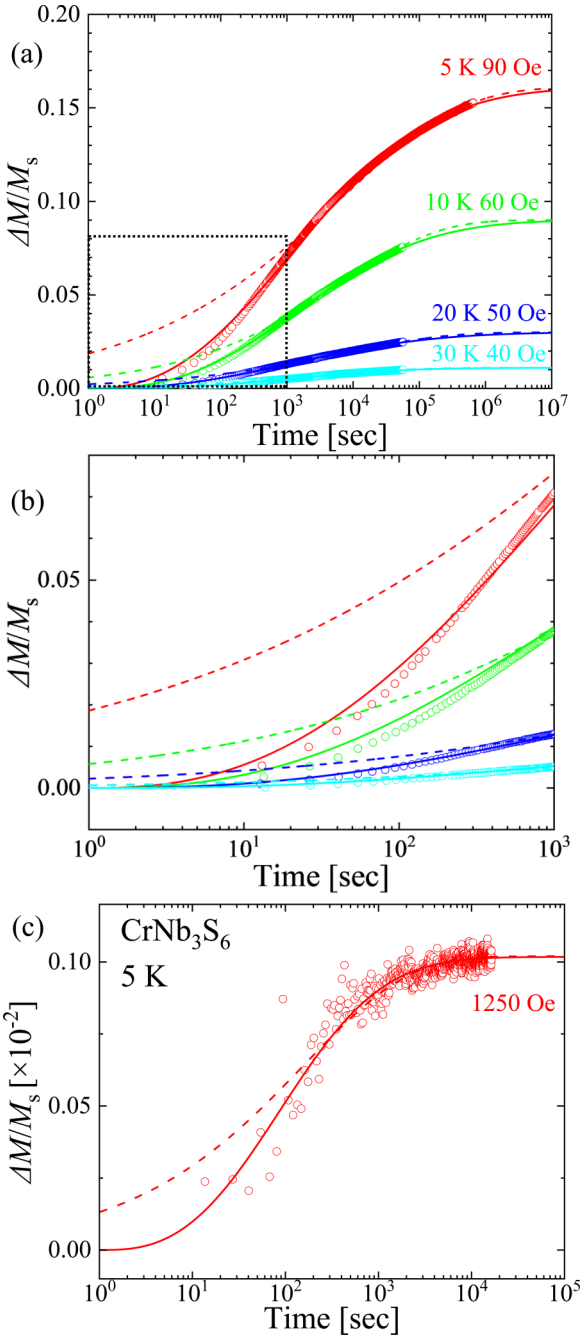

FIG. 10. (a) Time evolution of the M for the increasing H processes between 5 and 30 K on $MnNb_3S_6$. (b) Enlarged view of panel (a) for time less than 10^3 s. (c) Time evolution of the M for the increasing H process at 5 K on $CrNb_3S_6$. Both the data on $MnNb_3S_6$ and $CrNb_3S_6$ at 5 K are reproduced in Figs. 6(a) and 6(b), respectively. H was set between H_{c1} and H_{c2} at each T. The dashed and solid lines represent the results of the fitting by the stretched exponential function and Randeria's equation, respectively.

$MnNb_3S_6$ is the helical pitch. Our magnetic measurements and the previous neutron measurements suggest that $MnNb_3S_6$ stabilizes long-range CHM ordering, whose period is longer than that of $CrNb_3S_6$ [22]. The size of the solitons on $MnNb_3S_6$ is considered to be larger than that on $CrNb_3S_6$, so

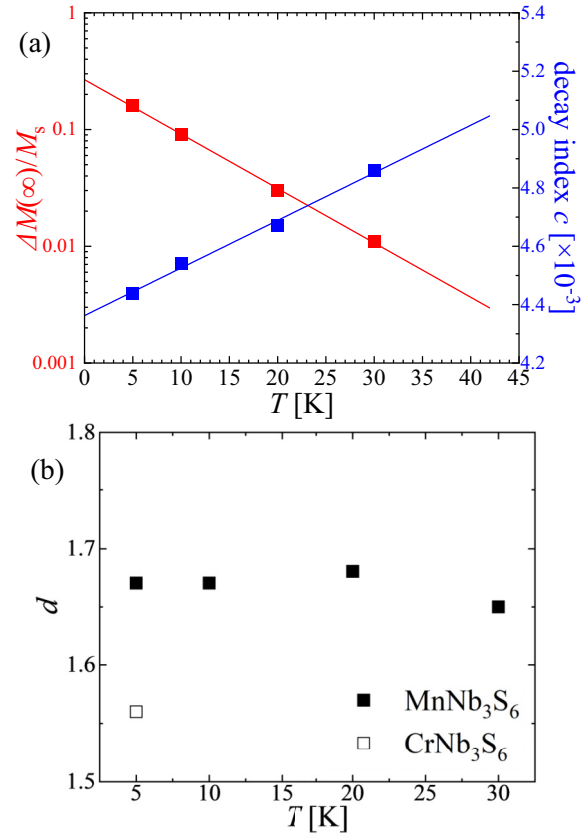

FIG. 11. (a) Temperature dependence of system dimension on $MnNb_3S_6$ and $CrNb_3S_6$. (b) Temperature dependence of $\Delta M(\infty)/M_s$ and decay index for $MnNb_3S_6$.

that the effective mass of solitons in $MnNb_3S_6$ is greater than that in $CrNb_3S_6$. In general, the magnetic relaxation time in a magnetic cluster increases as the size of the cluster increases. Therefore, the nonequilibrium state of the annihilation of the soliton on $MnNb_3S_6$ was detectable and enabled us to analyze the magnetization relaxation with good measurement accuracy through magnetic measurements.

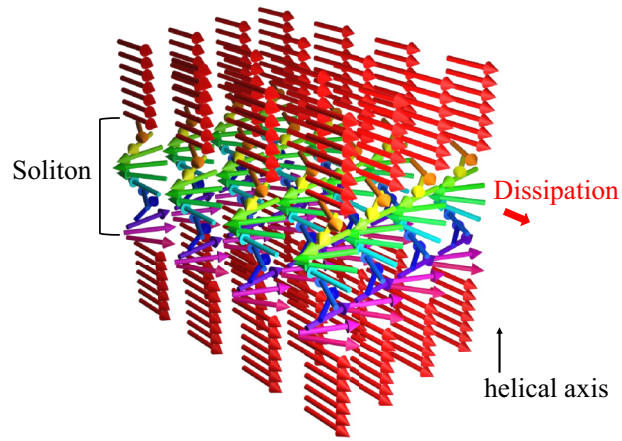

FIG. 12. Illustration of the annihilation process of the soliton cluster.

VI. CONCLUSION

In conclusion, we observed the characteristic magnetization process with magnetic field perpendicular to the *c* axis by the formation of the CSL on the bulk single crystal of $MnNb_3S_6$. The magnetization process of the CSL state had the large hysteresis. These results indicate that the long-range chiral helimagnetic state is stabilized. Furthermore, the magnetization relaxation accompanying the annihilation of the soliton was observed. The growth of the magnetization reached almost 16% of saturation magnetization in the process of the soliton annihilation. The annihilation process can be phenomenologically reproduced using the unfrustrated magnetic clusters model. A time-dependent microscopic analysis such as Lorentz TEM observation of CSL is desirable to confirm the nonequilibrium phenomenon visually.

ACKNOWLEDGMENTS

We thank Y. Nakao for helping sample preparation. We also thank Y. Kato for useful discussions. This work was supported by Grants-in-Aid for Scientific Research, Grant No. (S) 25220803, from the Ministry of Education, Culture, Sports, Science and Technology (MEXT), Japan. This work was also supported by JSPS KAKENHI (Grant No. 21H01799) and the Center for Chiral Science in Hiroshima University (the MEXT program for promoting the enhancement of research universities, Japan) and JSPS Core-to-Core Program, A. Advanced Research Networks.

[1] S. Mühlbauer, B. Binz, F. Jonietz, C. Pfleiderer, A. Rosch, A. Neubauer, R. Georgii, and P. Boni, Science **323**, 915 (2009).
[2] X. Z. Yu, Y. Onose, N. Kanazawa, J. H. Park, J. H. Han, Y. Matsui, N. Nagaosa, and Y. Tokura, Nature (London) **465**, 901 (2010).
[3] Y. Togawa, T. Koyama, K. Takayanagi, S. Mori, Y. Kousaka, J. Akimitsu, S. Nishihara, K. Inoue, A. S. Ovchinnikov, and J. Kishine, Phys. Rev. Lett. **108**, 107202 (2012).
[4] N. Nagaosa and Y. Tokura, Nat. Nanotechnol. **8**, 899 (2013).
[5] Y. Togawa, Y. Kousaka, K. Inoue, and J. Kishine, J. Phys. Soc. Jpn. **85**, 112001 (2016).
[6] I. E. Dzyaloshinskii, J. Phys. Chem. Solids **4**, 241 (1958).
[7] T. Moriya, Phys. Rev. **120**, 91 (1960).
[8] A. Neubauer, C. Pfleiderer, B. Binz, A. Rosch, R. Ritz, P. G. Niklowitz, and P. Böni, Phys. Rev. Lett. **102**, 186602 (2009).
[9] Y. Togawa, Y. Kousaka, S. Nishihara, K. Inoue, J. Akimitsu, A. S. Ovchinnikov, and J. Kishine, Phys. Rev. Lett. **111**, 197204 (2013).
[10] J. Kishine and A. Ovchinnikov, Solid State Phys. **66**, 1 (2015).
[11] T. Miyadai, K. Kikuchi, H. Kondo, S. Sakka, M. Arai, and Y. Ishikawa, J. Phys. Soc. Jpn. **52**, 1394 (1983).
[12] Y. Togawa, T. Koyama, Y. Nishimori, Y. Matsumoto, S. McVitie, D. McGrouther, R. L. Stamps, Y. Kousaka, J. Akimitsu, S. Nishihara, K. Inoue, I. G. Bostrem, V. E. Sinitsyn, A. S. Ovchinnikov, and J. Kishine, Phys. Rev. B **92**, 220412(R) (2015).
[13] K. Tsuruta, M. Mito, Y. Kousaka, J. Akimitsu, J. Kishine, Y. Togawa, H. Ohsumi, and K. Inoue, J. Phys. Soc. Jpn. **85**, 013707 (2016).
[14] M. Shinozaki, Y. Masaki, R. Aoki, Y. Togawa, and Y. Kato, Phys. Rev. B **97**, 214413 (2018).
[15] M. Mito, H. Ohsumi, K. Tsuruta, Y. Kotani, T. Nakamura, Y. Togawa, M. Shinozaki, Y. Kato, J. Kishine, J. Ohe, Y. Kousaka, J. Akimitsu, and K. Inoue, Phys. Rev. B **97**, 024408 (2018).
[16] M. Ohkuma, M. Mito, N. Nakamura, K. Tsuruta, J. Ohe, M. Shinozaki, Y. Kato, J. Kishine, Y. Kousaka, J. Akimitsu, and K. Inoue, AIP Adv. **9**, 075212 (2019).
[17] M. N. Wilson, E. A. Karhu, D. P. Lake, A. S. Quigley, S. Meynell, A. N. Bogdanov, H. Fritzsche, U. K. Rößler, and T. L. Monchesky, Phys. Rev. B **88**, 214420 (2013).
[18] S. A. Meynell, M. N. Wilson, H. Fritzsche, A. N. Bogdanov, and T. L. Monchesky, Phys. Rev. B **90**, 014406 (2014).
[19] A. O. Leonov and K. Inoue, Phys. Rev. B **98**, 054404 (2018).
[20] Y. Kousaka, Y. Nakao, J. Kishine, M. Akita, K. Inoue, and J. Akimitsu, Nucl. Instrum. Methods Phys. Res. Sect. A **600**, 250 (2009).
[21] S. Mankovsky, S. Polesya, H. Ebert, and W. Bensch, Phys. Rev. B **94**, 184430 (2016).
[22] S. K. Karna, F. N. Womack, R. Chapai, D. P. Young, M. Marshall, W. Xie, D. Graf, Y. Wu, H. Cao, L. DeBeer-Schmitt, P. W. Adams, R. Jin, and J. F. DiTusa, Phys. Rev. B **100**, 184413 (2019).
[23] S. K. Karna, M. Marshall, W. Xie, L. DeBeer-Schmitt, D. P. Young, I. Vekhter, W. A. Shelton, A. Kovács, M. Charilaou, and J. F. DiTusa, Nano Lett. **21**, 1205 (2021).
[24] A. E. Hall, J. C. Loudon, P. A. Midgley, A. C. Twitchett-Harrison, S. J. R. Holt, D. A. Mayoh, J. P. Tidey, Y. Han, M. R. Lees, and G. Balakrishnan, Phys. Rev. Mater. **6**, 024407 (2022).
[25] R. V. Chamberlin, G. Mozurkewich, and R. Orbach, Phys. Rev. Lett. **52**, 867 (1984).
[26] A. Ito, H. Aruga, E. Torikai, M. Kikuchi, Y. Syono, and H. Takei, Phys. Rev. Lett. **57**, 483 (1986).
[27] R. S. Freitas, L. Ghivelder, F. Damay, F. Dias, and L. F. Cohen, Phys. Rev. B **64**, 144404 (2001).
[28] A. Bhattacharyya, S. Giri, and S. Majumdar, Phys. Rev. B **83**, 134427 (2011).
[29] S. Ghara, B.-G. Jeon, K. Yoo, K. H. Kim, and A. Sundaresan, Phys. Rev. B **90**, 024413 (2014).
[30] H. Miyasaka, K. Nakata, L. Lecren, C. Coulon, Y. Nakazawa, T. Fujisaki, K.-i. Sugiura, M. Yamashita, and R. Clérac, J. Am. Chem. Soc. **128**, 3770 (2006).
[31] M. Mito, M. Ogawa, H. Deguchi, M. Yamashita, and H. Miyasaka, J. Appl. Phys. **107**, 124316 (2010).
[32] R. B. Griffiths, Phys. Rev. Lett. **23**, 17 (1969).
[33] M. Randeria, J. P. Sethna, and R. G. Palmer, Phys. Rev. Lett. **54**, 1321 (1985).
[34] A. J. Bray, Phys. Rev. Lett. **60**, 720 (1988).
[35] H. Oike, A. Kikkawa, N. Kanazawa, Y. Taguchi, M. Kawasaki, Y. Tokura, and F. Kagawa, Nat. Phys. **12**, 62 (2016).
[36] J. Wild, T. N. G. Meier, S. Pöllath, M. Kronseder, A. Bauer, A. Chacon, M. Halder, M. Schowalter, A. Rosenauer, J. Zweck, J. Müller, A. Rosch, C. Pfleiderer, and C. H. Back, Sci. Adv. **3**, e1701704 (2017).

[37] K. Karube, J. S. White, D. Morikawa, M. Bartkowiak, A. Kikkawa, Y. Tokunaga, T. Arima, H. M. Rønnow, Y. Tokura, and Y. Taguchi, Phys. Rev. Mater. **1**, 074405 (2017).

[38] M. T. Birch, R. Takagi, S. Seki, M. N. Wilson, F. Kagawa, A. Štefančič, G. Balakrishnan, R. Fan, P. Steadman, C. J. Ottley, M. Crisanti, R. Cubitt, T. Lancaster, Y. Tokura, and P. D. Hatton, Phys. Rev. B **100**, 014425 (2019).

[39] M. T. Birch, D. Cortés-Ortuño, N. D. Khanh, S. Seki, A. Štefančič, G. Balakrishnan, Y. Tokura, and P. D. Hatton, Commun. Phys. **4**, 1 (2021).

[40] J. Kishine, K. Inoue, and Y. Yoshida, Prog. Theor. Phys. Suppl. **159**, 82 (2005).

[41] A. L. Blanc-Soreau, J. Rouxel, M.-F. Gardette, and O. Gorochov, Mater. Res. Bull. **11**, 1061 (1976).

[42] Y. Dai, W. Liu, Y. Wang, J. Fan, L. Pi, L. Zhang, and Y. Zhang, J. Phys.: Condens. Matter **31**, 195803 (2019).

[43] Y. Dai, W. Liu, Y. Wang, J. Zhao, F. Meng, W. Tong, L. Pi, L. Zhang, and Y. Zhang, Appl. Phys. Lett. **117**, 022410 (2020).

[44] See Supplemental Material at http://link.aps.org/supplemental/10.1103/PhysRevB.106.104410 for ac magnetic measurements with varying ac frequency; magnetization relaxation measurements; soliton annihilation at 30 K; and fitting parameters.

[45] K. Tsuruta, M. Mito, Y. Kousaka, J. Akimitsu, J. Kishine, Y. Togawa, and K. Inoue, J. Appl. Phys. **120**, 143901 (2016).

[46] M. Ohkuma, M. Mito, Y. Kousaka, J. Akimitsu, J. Kishine, and K. Inoue, Appl. Phys. Lett. **118**, 132404 (2021).

[47] M. Ohkuma, M. Mito, Y. Kousaka, T. Tajiri, J. Akimitsu, J. Kishine, and K. Inoue, Appl. Phys. Lett. **117**, 232403 (2020).

[48] N. J. Ghimire, M. A. McGuire, D. S. Parker, B. Sipos, S. Tang, J.-Q. Yan, B. C. Sales, and D. Mandrus, Phys. Rev. B **87**, 104403 (2013).

[49] K. Tsuruta, M. Mito, H. Deguchi, J. Kishine, Y. Kousaka, J. Akimitsu, and K. Inoue, Phys. Rev. B **93**, 104402 (2016).